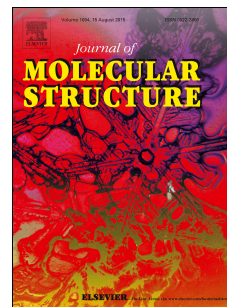


# Accepted Manuscript

Crystal structure, vibrational spectra, optical properties and density functional theory approach of a picrate salt based on substituted triphenylphosphinium

Ting Li, Zhi-Hao Gan, Cai-Hong Liu, Jia-Rong Zhou, Xiao-Ping Liu, Le-Min Yang, Chun-Lin Ni



PII: S0022-2860(18)31416-9

DOI: <https://doi.org/10.1016/j.molstruc.2018.11.103>

Reference: MOLSTR 25932

To appear in: *Journal of Molecular Structure*

Received Date: 21 February 2018

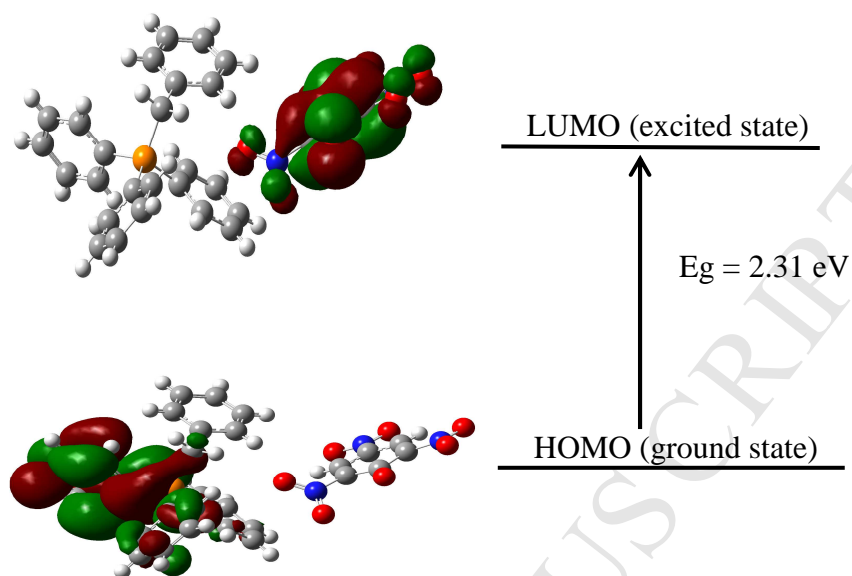
Revised Date: 7 September 2018

Accepted Date: 28 November 2018

Please cite this article as: T. Li, Z.-H. Gan, C.-H. Liu, J.-R. Zhou, X.-P. Liu, L.-M. Yang, C.-L. Ni, Crystal structure, vibrational spectra, optical properties and density functional theory approach of a picrate salt based on substituted triphenylphosphinium, *Journal of Molecular Structure* (2018), doi: <https://doi.org/10.1016/j.molstruc.2018.11.103>.

This is a PDF file of an unedited manuscript that has been accepted for publication. As a service to our customers we are providing this early version of the manuscript. The manuscript will undergo copyediting, typesetting, and review of the resulting proof before it is published in its final form. Please note that during the production process errors may be discovered which could affect the content, and all legal disclaimers that apply to the journal pertain.

## Graphical Abstract-Pictogram



# Crystal structure, vibrational spectra, optical properties and density functional theory approach of a picrate salt based on substituted triphenylphosphinium

Ting Li, Zhi-Hao Gan, Cai-Hong Liu, Jia-Rong Zhou\*, Xiao-Ping Liu, Le-Min Yang, Chun-Lin Ni\*

*College of Materials and Energy, Institute of Biomaterial, South China Agricultural University, Guangzhou 510642, P. R. China*

**Abstract:** A new organic crystal, [BzTPP][PIC](1) ([BzTPP]<sup>+</sup> = benzyl triphenylphosphinium, [PIC]<sup>-</sup> = picrate), has been grown by slow evaporation solution growth technique. Single crystal XRD reveals that it belongs to monoclinic system with  $P2_1/c$ . The two neighboring [BzTPP]<sup>+</sup> cations form a dimer through C-H... $\pi$  interaction while anions stack into a columnar structure through N...O, O...O and  $\pi$ ... $\pi$  interaction. The anions and cations form a column structure alternately in ...AC-AC-AC-AC... sequence through C-H...O hydrogen bonds. The experimental vibrational bands (IR and Raman) have been discussed and assigned based on DFT calculations. The HOMO-LUMO energy gap explains the charge transfer interactions in the molecule. The thermal stability of the hybrid crystal was analyzed by TG-TDA-MS technique and revealed that the title crystal was stable up to 290 °C. The fluorescence spectra reveal three main emission peaks at 295, 388 and 543 nm upon excitation at 250 nm in solid state at room temperature. The energy of weak interactions in the molecule and nonlinear optical properties were studied using DFT calculations.

**Keywords:** Substituted benzyl triphenylphosphinium picrate; Crystal structure; vibrational spectra; Optical properties; DFT calculations.

---

\*Corresponding author.

E-mail address: scau534@126.com (Jia-Rong Zhou); [niclchem@scau.edu.cn](mailto:niclchem@scau.edu.cn) (Chun-Lin Ni)

## 1. Introduction

New nonlinear optical materials have been attracting much attention in recent researches due to their potential applications in many optical fields [1-5]. Compared to the inorganic materials, organic materials not only own delocalized  $p$ -electrons with conjugated double bond systems but also show excellent properties such as high optical quality, superior long-term orientation, high packing densities and larger photo-chemical stabilities, etc [6-9]. Organic crystals also possess unsatisfactory poor thermal and mechanical properties for they are usually formed through weak van der Waals forces [10-12]. In order to overcome the limitations of those materials, the design and preparation of hybrid materials from organic electron donor-acceptor system have been implemented to improve their chemical and thermal stability, mechanical strength and optical non-linearity [13-16]. It is well known that the picric acid (2,4,6-trinitrophenol) acts not only as an acceptor but also acidic ligand and has strong tendency to form the hydrogen bonds with other compounds [17-20]. On the one hand, picric acid is famous as an electron acceptor forming charge transfer molecular complexes with a number of electron donor compounds through electrostatic or hydrogen bond interactions [19, 20]. On the other hand, picric acid has the ability to form ionic bonds with basic amino acids and may also form dissociable charge-transfer complexes with suitable for aromatic group [21-23]. These outstanding properties make them suitable for industrial chemical application in the processes of the dye, leather and glass industry [24, 25]. According to our previous work, several researches on the inorganic-organic hybrid materials containing triphenylphosphinium cations and anions containing metal atoms have been done such as  $[\text{BzTPP}]_2[\text{Co}(\text{NCS})_4]$  which exhibits a magnetic coupling interaction from ferromagnetic to antiferromagnetic around 30 K as the temperature is lowered [26], and

[BzTPP][Ni(mnt)<sub>2</sub>] the adjacent cations of which are connected together via  $\pi$ - $\pi$  interaction between the conjugated phenyl rings of [BzTPP]<sup>+</sup> cation [27]. Despite recent efforts, the synthesis of defined crystalline materials is still far from rational and typically relies on spontaneous. Hence, the synthesis of defined building blocks and studies of their structural properties are desirable in order to provide a sound base for their subsequent use in the preparation of crystalline materials. Taking the outstanding properties of picric acid and [BzTPP]<sup>+</sup> cations into consideration, thus in the present work we introduce picric acid instead of the metal anions mentioned above into the system of [BzTPP][M(mnt)<sub>2</sub>](M = Cu, Ni), combining with benzyltriphenylphosphonium. Herein, as shown in Fig. 1, a new picric salt, [BzTPP][PIC](1), was designed and investigated by means of single crystal XRD, IR, Raman, UV-visible and fluorescence spectroscopy, and thermal and nonlinear optical analysis.

## 2. Experimental

### 2.1 General materials

Picric acid, K<sub>2</sub>CO<sub>3</sub>, benzyl bromide, triphenylphosphine and all solvents were purchased from commercial sources and used without further purification. All manipulations were performed in air. Benzyl triphenylphosphonium bromide was synthesized following the literature procedure [28].

### 2.2 Synthesis of the title crystal

A methanol solution (10 mL) of picric acid (0.23 g, 1.0 mmol) was added to the methanol solution (10 mL) of K<sub>2</sub>CO<sub>3</sub> (0.07 g, 0.5 mmol) and stirred violently for 2 hours at room temperature, and 20 mL methanol solution of [BzTPP]Br (0.43 g, 1.0 mmol) were dropped to the mixture, and stirred for another 1 h. The yellow precipitate was filtered off, then washed with

methanol and ether, and dried in vacuum. Yield 78 %. *Anal.* Calc. for  $C_{31}H_{34}PN_3O_7$ : C, 64.11; H, 4.27; N, 7.18 %; Found: C, 64.03; H, 4.16; N, 7.23 %.

### 2.3 Physical Measurements

Elemental analyses (C, H and N) were recorded on an Elementar Vario EL III instrument. Infrared spectra were recorded on a Nicolet Nexus 670 FT-IR spectrophotometer in the range 4000 to 400  $cm^{-1}$  with the samples in the form of KBr pellets. Raman spectra were recorded in the region of 3500-400  $cm^{-1}$  on a Thermo-Fisher Nicolet NXR 9650 FT-Raman spectrometer, and the excitation wavelength is 1064 nm. Electronic spectra were recorded on a SHIMADZU UV-3150 spectrophotometer in the range 600 to 200 nm in  $CH_3OH$ . Solid-state UV-Vis absorption and transmission spectra were recorded on a Shimadzu UV-2550 spectrophotometer in the region of 200-450 nm. Solid-state emission spectra were recorded for the solid samples which were loaded into a sample cell (1cm diameter) which was then fixed on a bracket at room temperature with a Shimadzu RF-5301PC fluorescence spectrophotometer. The excitation and emission slits used for the measurement of the solid state of the crystals were 2.5 and 5.0 nm wide, the scan speed was 240  $nm \cdot min^{-1}$ , and the scan voltage was 500V. The X-ray powder diffraction (XRPD) data were collected by a Rigaku Corporation D/MAX2200VPC using Cu  $K\alpha$  radiation ( $\lambda = 1.5406 \text{ \AA}$ ). Thermogravimetric (TG), differential thermal analyses (DTA) and mass spectra (MS) of the gaseous products of the decomposition for the title compound were carried out on a Rigaku Thermo Mass Photo TG-MS analyzer at a heating rate of  $10^\circ C \text{ min}^{-1}$  in the temperature range of 30-800 $^\circ C$  in a helium atmosphere.

### 2.4 Determination of crystal structure

Yellow single crystals suitable for the X-ray structure analysis were obtained by evaporating

the solution of **1** in MeOH for three weeks at room temperature. A photograph of the as-grown crystals of **1** is shown in Fig. 2. Diffraction data were collected at 291 K with a Bruker Smart APEX CCD diffractometer using graphite-monochromated Mo K $\alpha$  radiation ( $\lambda = 0.71073 \text{ \AA}$ ) and operating in  $\omega$ - $\phi$  scan mode. Cell parameters of **1** were obtained and refined using the SAINT [29] program. The structures were solved by direct methods using the SHELXS-97 [30] program, and refined on  $F^2$  by full-matrix least-squares methods using the SHELXTL-97 [31] program for all non-hydrogen atoms. All hydrogen atoms were introduced in calculated positions and refined with fixed geometry with respect to their carrier carbon atoms. Crystal data, data collection and refinement details for **1** are given in Table 1. Selected bond parameters for **1** are listed in Table 2.

### 2.5 Computational Details

All calculations were carried out using the Gaussian 09 programs [32]. The ground state geometries of molecules were obtained from optimizations using the B3LYP functional [33, 34] with the 6-31G (d, p) basis set. Frequency analysis was used to confirm whether the structure is a minimum (with no imaginary frequency) and to provide IR and Raman spectra. A TD-DFT calculation was carried out to obtain UV-Vis absorption spectrum. Non-linear optical properties of the title crystal were studied using DFT calculations. Since the values of the polarizability and hyperpolarizability given by Gaussian 09 are reported in atomic units (a.u.), the calculated values have been converted into electrostatic units (esu) ( $\alpha_{ij}$ : 1 a.u. =  $0.1482 \times 10^{-24}$  esu;  $\beta_{ijk}$ : 1 a.u. =  $8.3693 \times 10^{-33}$  esu).

## 3. Results and discussion

### 3.1 Description of crystal structure and interaction energy

The title salt [BzTPP][PIC](**1**) crystallizes in the monoclinic system, space group  $P2_1/c$ . As

shown in Fig. 3, the asymmetric unit is comprised of one [BzTPP]<sup>+</sup> cation and one picrate monoanion. The [BzTPP]<sup>+</sup> cation adopts a conformation in which four phenyl rings are twisted relative to C(12)-C(13)-P(1) reference plane, with dihedral angles of 95.8°(2) ( $\theta_1$ ) for C(7)-C(12), 75.6°(2) ( $\theta_2$ ) for C(14)-C(19), 150.3°(1) ( $\theta_3$ ) for C(20)-C(25) and 95.6°(2) ( $\theta_4$ ) for C(26)-C(31) rings respectively. It is observed that the adjacent [BzTPP]<sup>+</sup> cations form a dimer through the C-H... $\pi$  interactions with a H(29)-C<sub>g1</sub>(C<sub>g1</sub> is center of C(24)-C(29) ring) distance of 2.956 Å (Fig. 4a). For the picrate anion moiety, the loss of a proton from the picric results in the lengthening of the C(1)-O(1) bond with a distance of 1.233(4) Å [21]. In addition, the C(1)-C(2)(1.450 Å) and C(1)-C(6) (1.453 Å) distances are both longer than the normal aromatic C-C values 1.4 Å [35] due to the loss of a hydroxyl proton at O(1) leading to the conversion from the neutral to anionic state. Meantime the neighboring anions adjoin together forming a columnar (Fig. 4b) through the interactions of O...O, N...O and  $\pi$ ... $\pi$  with distances of 3.486(2) Å, 3.408(3) Å and 3.618 (3) Å, respectively [22].

The inter-molecular energy calculations were performed using the Gaussian 03 package at the DFT/B3LYP/6-31G (d, p) level in order to understand various interactions such as electrostatic interaction, hydrogen bonds in [BzTPP]<sup>+</sup> cation and [PIC]<sup>-</sup> anion (Fig. 4c). The total energy for the intermolecular interaction was calculated to be -45.7 Kcal/mol. The detailed parameters about of these hydrogen bonds were listed in Table 3. The packing diagram of **1** along the crystallographic *a*-axis direction is displayed in Fig. S1. The crystal packing is governed by these hydrogen bonds which may be effective in the stabilization of the crystal structure.

### 3.2 Powder X-ray diffraction

The simulated and experimental PXRD patterns of **1** are shown in Fig. 5. The PXRD pattern

fits quite well with simulated one, therefore bulk material purity is confirmed. So the powder sample of the material was suitable for the measurement of spectral and optical properties.

### 3.3 Thermal stability

The TG and DTA curves of **1** are presented in Fig. 6. From TG curve, it is clear that there is no obvious weight loss between room temperature to 308 °C and hence it shows that the [BzTPP][PIC] crystal is stable up to 308 °C. TG curve indicates two stage mass loss patterns when the material was heated from 30 and 800 °C. The first decomposition was started at 308 and ended at 355 °C with the loss of w98.3% of material. The next weight loss occurs between 355 °C and 800 °C with the removal of w1.7% of material. It is noted when the decomposition process was carried up to 800 °C with the removal of the material into gaseous products [36]. The sharp endothermic peak observed in DTA curve at 308 °C shows the melting point of the material, and the another peak observed in DTA is in consistence with the TG curve. It is fully stable only up to 308 °C so that it can be used for NLO applications up to this temperature.

The gaseous products of the decomposition of [BzTPP][PIC] at ~308 °C were determined by mass spectra as shown in Fig. S2. As can be seen from the m/z data, the main gaseous matters were H<sub>2</sub>O (m/z = 18), N<sub>2</sub> (m/z = 28), CO<sub>2</sub> (m/z = 44) from the decomposition of [PIC]<sup>-</sup> anion; C<sub>3</sub>H<sub>3</sub><sup>+</sup> (m/z = 39), C<sub>4</sub>H<sub>4</sub><sup>+</sup> (m/z = 51), C<sub>5</sub>H<sub>5</sub><sup>+</sup> (m/z = 65), and C<sub>6</sub>H<sub>5</sub><sup>+</sup> (m/z = 77), and PhCH<sub>2</sub><sup>+</sup> (m/z = 91) from the decomposition of [BzTPP]<sup>+</sup> cation.

### 3.4 IR and Raman spectra

The FT-IR spectra for **1** in 4000-500 cm<sup>-1</sup> region are shown in Fig. 7a, while Fig. 7b shows spectra Raman spectra in 3500-400 cm<sup>-1</sup> region. The theoretical FT-IR and Raman spectra of [BzTPP]<sup>+</sup> cation and [PIC]<sup>-</sup> anion are shown in Figs. S3 and S4, respectively. And the observed

experimental and theoretical of IR and Raman bands frequencies and assignments are given in Table S1.

In the moiety of the [BzTPP]<sup>+</sup> cation. The peaks at 3062 cm<sup>-1</sup> in the IR spectra and 3063 cm<sup>-1</sup> in the Raman spectra are assigned to the stretching vibration of the C-H bonds in the benzenyl ring, the calculated peaks are located at 3262 cm<sup>-1</sup>(IR) and 3267 cm<sup>-1</sup>(Raman), respectively. The peaks occur at 2954, 2918 cm<sup>-1</sup> in the IR spectra and 2969, 2912 cm<sup>-1</sup> in the Raman assigned as the C-H vibration of -CH<sub>2</sub> group of the benzyl group. The peaks at 1630, 1558, 1485 cm<sup>-1</sup> (IR) and 1571, 1480 cm<sup>-1</sup>(Raman) are due to the C=C vibration of the phenyl ring showing great agreement with the theoretic values, these mode are computed at 1650, 1591, 1480 cm<sup>-1</sup> (IR) and 1640, 1596, 1475 cm<sup>-1</sup> (Raman). The asymmetric vibration of CH<sub>2</sub> group appears at 1429 cm<sup>-1</sup> (IR), calculated at 1413 cm<sup>-1</sup> (IR) and 1408 cm<sup>-1</sup> (Raman). The bending ( $\delta$ NO<sub>2</sub>) mode give rises to the band present at 1330 cm<sup>-1</sup> (IR), which have great similarities in the DFT, more explicitly, 1373 cm<sup>-1</sup> (DFT) in both IR and Raman spectra. As the same time, the rocking pCH<sub>2</sub> mode are observed at 1186, 1155, 1113, 912 cm<sup>-1</sup> (IR) and 1191, 1153, 1101, 912 cm<sup>-1</sup> (Raman), 1190, 1156, 1114, 919 cm<sup>-1</sup> (IR, DFT), 1256, 1114, 923 cm<sup>-1</sup> (Raman, DFT). The C-P characteristic peak is discovered at 751 cm<sup>-1</sup>(IR) and 755 cm<sup>-1</sup> (Raman), the DFT of IR and Raman are recorded in 767 cm<sup>-1</sup> (IR) and 762 cm<sup>-1</sup>.

As the portion of [PIC]<sup>-</sup> anion, the main characteristic vibrations show great relationships with the nitro group. Means, the groups of -NO<sub>2</sub> have characteristic vibration active in both IR and Raman spectra. The most intense lines in the 1315 (IR) and 1310 cm<sup>-1</sup> (Raman) are owing to the symmetric stretching vibration of nitro group ( $\nu_s$ NO<sub>2</sub>) and are characteristic of the picrate anion, calculated at 1311 cm<sup>-1</sup>(IR) and 1307 cm<sup>-1</sup> Raman. The asymmetric stretching vibration of nitro

groups sit at 1558, 1552  $\text{cm}^{-1}$  (IR) 1571  $\text{cm}^{-1}$  (Raman), 1591, 1529  $\text{cm}^{-1}$  (DFT, IR) and 1596  $\text{cm}^{-1}$  (DFT, Raman). The bending in plane ( $\delta\text{NO}_2$ ), wagging ( $\omega\text{NO}_2$ ), scissoring ( $\phi\text{NO}_2$ ), rocking ( $\rho\text{NO}_2$ ) vibration mode of nitro groups are assigned at nearby  $\sim 800 \text{ cm}^{-1}$ ,  $\sim 740 \text{ cm}^{-1}$ ,  $710 \text{ cm}^{-1}$  and  $530 \text{ cm}^{-1}$ .<sup>[4, 19]</sup> Peaks of  $1155 \text{ cm}^{-1}$  in IR and  $1101 \text{ cm}^{-1}$  in Raman are ascribed to the phenolic O and the main characteristic of the picrate anion [24]. Those vibration mode shows good agreement with the theoretic values calculated in the DFT, showing in the Table 4.

### 3.5 UV-vis and transmittance spectra analysis

The electronic absorption spectrum of [BzTPP][PIC] shows two strong absorption bands at 245 and 373 nm in Fig. 8a. The strong absorption band at 373 nm, is attributed to  $\pi\text{-}\pi^*$  transition of picrate ion, accompanying a slight blue shift at 375 nm compared with previously reported compound [37], which indicated that there is a charge activity in compound **1** as a consequence of C-O group transition and delocation in the benzene of picrate and triphenylphosphine [1, 38]. To support experimental observations, the theoretical absorption wavelengths and electronic excitation energies were calculated by the TD-DFT method. The calculations predicts two intense electronic transition at 247 and 363 nm of the [BzTPP]<sup>+</sup> cation and 375 nm of the [PIC]<sup>-</sup> anion (Fig. S5), which are similar to the measured experimental data (245 and 373 nm). The highest occupied molecular orbitals and lowest unoccupied molecular orbitals of [BzTPP][PIC] are shown in Fig. 8b. The orbital that primarily acts as an electron donor is the HOMO, while is the orbital that mainly acts as an electron acceptor is the LUMO. The energy gap of 2.31eV explains the eventual charge transfer interactions taking place in the material [39].

The recorded transmittance spectrum is shown in Fig. 8c and it has good transparency of about 63% with lower cut-off wavelength 465 nm. The lower cut-off wavelength is due to the

$\pi$ - $\pi^*$  transition of the phenyl group of the title compound [40]. The yellow crystal of **1** is active in the visible region, indicating potential application as optical material. When wavelength is more than 465 nm, the reflection ability of the material increases exponentially, and tends to be stable when the wavelength is more than 540 nm.

### 3.6 Fluorescence properties

The luminescent properties of title compound and the corresponding intermediate [BzTPP]Br were investigated in solid state at room temperature. As shown in Fig. 9 upon excitation at 250 nm, the intermediate [BzTPP]Br shows main luminescent emissions peaks at 390, 466 and 543 nm with a weaker shoulder emission peak at 309 nm. There also exists three peaks at 543, 388 and 295 nm in the compound **1**, more explicitly, the maximum emission peak changes from 390 to 388 nm with an slightly blue-shifted of 2 nm, the peak at 309 changes to 295 nm with blue-shifted of 15 nm when the intermediate [BzTPP]Br is combined with the self-assembly priciate anion and formed [BzTPP][PIC] molecular solid. The difference of locations of peaks and the change of the intensity may be a result of C-H $\cdots$ N weak interactions between the [BzTPP]<sup>+</sup> anion and [PIC]<sup>-</sup> cation and the neighboring anions forming of a column [22, 41].

### 3.7 NLO properties

The electric dipole moment ( $\mu_i$ ), polarizability ( $\alpha_{ij}$ ) and the first hyperpolarizability ( $\beta_{ijk}$ ) of the [BzTPP][PIC] calculated by the B3LYP/6-31G(d, p) are listed in Table S2. The calculated dipole moment is equal to 31.90 D. The highest absolute value of the dipole moment is observed for the component  $\mu_x$ . In this direction, the value is equal to 31.81. The calculated polarizability ( $\alpha_{tot}$ ), is equal to  $52.99 \times 10^{-24}$  esu. As we can see, the first hyperpolarisability ( $\beta_{tot}$ ) of the compound has for value  $109.58 \times 10^{-31}$  esu, which is about 16 times that of the reference crystal KDP ( $\beta_{KDP} =$

$6.85 \times 10^{-31}$  esu). The above results show that the [BzTPP][PIC] is a good material for NLO applications. Also, it is remarkable, according to Table 4, that the value of the hyperpolarizability of the [BzTPP][PIC] cluster is distinctly larger than that of the picrate anion and the [BzTPP]<sup>+</sup> cation, which shows that the interactions between the anion and the cation play an important role not only in the generation of the crystal structure and its stability, but also in the enhancement of its optical properties [42].

#### 4. Conclusion

A new organic crystal of benzyl triphenylphosphinium picrate was synthesized, and the single crystals were grown by a slow evaporation method. The crystal structural analysis shows that the anions stack into a columnar structure through N $\cdots$ O, O $\cdots$ O and  $\pi\cdots\pi$  interaction, while the two neighboring [BzTPP]<sup>+</sup> cations form a dimer through C-H $\cdots\pi$  interaction. The anions and cations form a column structure alternately in  $\cdots$ AC-AC-AC-AC $\cdots$  sequence through C-H $\cdots$ O hydrogen bonds. The powder X-ray diffraction study confirms that the crystalline perfection is fairly good. The thermal stability and the main gaseous products of the decomposition of [BzTPP][PIC] at 308 °C of the hybrid crystal was analyzed by TG-TDA-MS technique and revealed that the title crystal was stable up to 220 °C. The experimental vibrational bands (IR and Raman) have been discussed and assigned based on DFT calculations. The HOMO-LUMO energy gap explains the charge transfer interactions in the molecule. The fluorescence spectra reveal three main emission peaks at 295, 388, and 543 nm upon excitation at 250 nm in solid state at room temperature. The energy of weak interactions in the molecule and nonlinear optical properties were studied using DFT calculations and reveal the first hyperpolarisability ( $\beta_{\text{tot}}$ ) of the crystal is about 16 times that of the reference crystal KDP. So, from the present investigation, it is concluded that [BzTPP][PIC]

is a new candidate for NLO device application.

### Supplementary material

Crystallographic data for the structural analysis of **1** have been deposited with the Cambridge Crystallographic Data Centre, CCDC No. 1468873. Copies of this information may be obtained free of charge from the Director, CCDC, 12 Union Road, Cambridge, CB2 1EZ, UK (fax: +44-1223-336033; deposit@ccdc.cam.ac.uk or www: <http://www.ccdc.cam.ac.uk>).

### Acknowledgements

This work has been partially supported by the Science and Technology Project (2016A010103025) from Guangdong Science and Technology Department, and the Undergraduates' Innovative Experimental Program (No.1056411137) in University from South China Agricultural University.

### References

- [1] K. Senthil, S. Kalainathan, A. R. Kumar, P.G. Aravindan, Investigation of synthesis, crystal structure and third-order NLO properties of a new stilbazolium derivative crystal: a promising material for nonlinear optical devices, *RSC Adv.* 4 (2014) 56112-56127.
- [2] S. Guidara, H. Feki, Y. Abid, Vibrational spectral studies and non-linear optical properties of L-leucine L-leucinium picrate: A Density Functional Theory approach, *Spectrochim. Acta A* 115 (2013) 437-444.
- [3] C. Zhang, Y. L. Song and X. Wang, Correlations between molecular structures and third-order non-linear optical functions of heterothiometallic clusters: a comparative study, *Coord. Chem. Rev.* 251 (2007) 111-141.
- [4] Z. Sun, X. Liu, X. Wang, L. Li, X. Shi, S. Li, C. Ji, J. Luo, M. Hong, Engineering of acentric stilbazolium salts with large second-order optical nonlinearity and enhanced environmental stability, *Cryst. Growth Des.* 12 (2012) 6181-6187.
- [5] V. Ramesh, K. Rajarajam, Crystal growth and characterization of a novel inorganic-organic hybrid NLO

- crystal:  $(\text{NH}_4)[\text{Cd}(\text{NCS})_3] \cdot \text{C}_{12}\text{H}_{24}\text{O}_6$ , *Appl. Phys. B* 113 (2013) 99-106.
- [6] B. J. Coe, J. A. Harris, I. Asselberghs, K. Wostyn, K. Clays, A. Persoons, B. S. Brunschwig, S. J. Coles, T. Gelbrich, M. E. Light, M. B. Hursthouse and K. Nakatani, Quadratic optical nonlinearities of N-methyl and N-aryl Pyridinium salts, *Adv. Funct. Mater.* 13 (2003) 347-357.
- [7] Y. Takahashi, H. Adachi, T. Taniuchi, M. Takagi, Y. Hosokawa, S. Onzuka, S. Brahadeeswaran, M. Yoshimura, Y. Mori, H. Masuhara, T. Sasaki and H. J. Nakanishi, Organic nonlinear optical DAST crystals for electro-optic measurement and terahertz wave generation, *J. Photochem. Photobiol.* 183 (2006) 247-252.
- [8] G. Seetharam Shettigar, K. Umesh, K. Chandrasekharan and Balakrishna Kalluraya, Investigation of synthesis, crystal structure and third-order NLO properties of a new stilbazolium derivative crystal: a promising material for nonlinear optical devices, *Synth. Met.* 57 (2007) 142-146.
- [9] J. Zyss, *Molecular nonlinear optics: materials, physics, and devices*, Academic press, 2013.
- [10] A. Kandasamy, R. Siddeswaran, P. Murugakoothan, P.S. Kumar, R. Mohan, Cellular localization of stem cell factor and c-kit receptor in the mouse nervous system, *Cryst. Growth Des.* 7 (2007) 183-186.
- [11] K.M. Priyadarshimi, A. Chandramohan, G.A. Badu, P. Ramasamy, Synthesis, crystal growth, spectral, optical, thermal and dielectric studies of dichloro (4-hydroxy-L-proline) cadmium (II) single crystals, *Optik* 125 (2014) 1390-1395.
- [12] B. Uma, R.K. Sakthi Murugesan, S. Krishnan, B.M. Boaz, Growth, structural, optical, thermal and dielectric properties of a novel semi-organic nonlinear optical crystal: Dichloro-diglycine zinc II, *Prog. Nat. Sci. Mater. Int.* 24 (2014) 378-387.
- [13] J. J. Bergkamp, S. Decurtins, S. X. Liu, Current advances in fused tetrathiafulvalene donor-acceptor systems, *Chem. Soc. Rev.* 44 (2015) 863-874.
- [14] Y. X. Zhao, J. R. Swierk, J. D. Megiatto Jr, B. Sherman, W. J. Youngblood, D. D. Qin, D. M. Lentz, A. L.

- Moore, T. A. Moore, D. Gust, T. E. Mallouk. Improving the efficiency of water splitting in dye-sensitized solar cells by using a biomimetic electron transfer mediator, *Proc. Nat. Acad. Sci. USA* 109 (2012) 15612-15616.
- [15] T. Bessho, S. M. Zakeeruddin, C.Y. Yeh, E. W. G. Diau, M. Grtzel, Highly Efficient Mesoscopic Dye-Sensitized Solar Cells Based on Donor-Acceptor-Substituted Porphyrins, *Angew. Chem. Int. Ed.* 49 (2010) 6646-6649.
- [16] P. M. Beaujuge, C. M. Amb, J. R. Reynolds, Spectral engineering in  $\pi$ -conjugated polymers with intramolecular donor- acceptor interactions, *Accounts Chem. Res.* 43 (2010) 1396-1407.
- [17] S. Ebert, P. Fischer, H. J. Knackmuss, Converging catabolism of 2, 4, 6-trinitrophenol (picric acid) and 2, 4-dinitrophenol by *Nocardioides simplex* FJ2-1A, *Biodegradation* 12 (2001) 367-376.
- [18] P.G. Thorne, Thomas.F. Jenkins, A field method for quantifying ammonium picrate and picric acid in soil, *Field Anal Chem. & Tech.* 1 (1997) 165-170.
- [19] K. Muthu, Subbiah Meenakshisundaram, Crystal growth, structure and characterization of *p*-Toluidinium picrate, *J. Cryst. Growth* 352 (2012) 163-166.
- [20] V. Tomasi, N. Biliskov, T. Mihelj, Z. Stefani, Thermal behaviour and structural properties of surfactant-Picrate compounds: The effect of the ammonium headgroup number, *Thermochim. Acta* 569 (2013) 25-35.
- [21] B. I. M. Cooke, J. M. Diamond, A. D. Grinnell, S. Hgaiwara, H. Sakata, Suppression of the action potential in nerve by nitrobenzene derivatives, *Physiology* 60 (1968) 470-477.
- [22] N. Goel, U. P. Singh, G. Singh, P. Srivastava, Study of picrate salts with amines, *J. Mol. Struct.* 1036 (2013) 427-438.
- [23] M. A. F. Elmosallamy, New highly selective picrate sensors based on charge-transfer complexes, *Anal. Sci.* 2004, 20 (2004) 285-290.

- [24] S. Suguna, D. Anbuselvi, D. Jayaraman, K. S. Nagaraja, B. Jeyaraj, Synthesis, growth, structural and optical studies of organic nonlinear optical material–Piperazine-1, 4-dium bis 2, 4, 6-trinitrophenolate, *Spectrochim. Acta A* 132 (2014) 330-338.
- [25] Y. X. Yan, X. T. Tao, Y. H. Sun, G. B. Xu, C. K. Wang, J. X. Yang, X. Zhao, Y. Z. Wu, Y. Ren, M. H. Jiang, Two new asymmetrical two-photon photopolymerization initiators: Synthesis, characterization and nonlinear optical properties, *Opt. Mater.* 27 (2005) 1787-1792.
- [26] X. Chen, W. Q. Chen, S. Han, J. F. Liu, J. R. Zhou, L. L. Yu, L. M. Yang, C. L. Ni, X. L. Hu, Two hybrid materials self-assembly from tetra (isothiocyanate) cobalt (II) dianion and substituted benzyl triphenylphosphonium, *J. Mol. Struct.* 984 (2010) 164-169.
- [27] C. L. Ni, Y. Z. Li, Q. J. Meng, Synthesis, crystal structure and magnetic properties of a new ion-pair complex benzyltriphenylphosphonium-bis (maleonitriledithiolato) nickel, *J. Coord. Chem.* 58 (2005) 759-766.
- [28] R. Broos, M. Anteunis, A simplified Wittig synthesis of substituted styrenes, *Synth. Commun.* 6 (1976) 53-57.
- [29] SMART, version 6.1, Bruker molecular analysis research tool; Bruker AXS: Madison, WI, 2000.
- [30] SAINTPlus, version 6.01, Data reduction and correction program; Bruker AXS: Madison, WI, 2000.
- [31] SHELXTL, Version 6.10. Structure determination software programs; Sheldrick, G. M. Bruker AXS Inc.; Madison, WI, 2000.
- [32] M. J. Frisch, G. W. Trucks, H. B. Schlegel, G. E. Scuseria, M. A. Robb, J. R. Cheeseman, G. Scalmani, V. Barone, B. Mennucci, G. A. Petersson, H. Nakatsuji, M. Caricato, X. Li, H. P. Hratchian, A. F. Izmaylov, J. Bloino, G. Zheng, J. L. Sonnenberg, M. Hada, M. Ehara, K. Toyota, R. Fukuda, J. Hasegawa, M. Ishida, T. Nakajima, Y. Honda, O. Kitao, H. Nakai, T. Vreven, J. A. Montgomery, Jr., J. E. Peralta, F. Ogliaro, M. Bearpark, J. J. Heyd, E. Brothers, K.N. Kudin, V.N. Staroverov, R. Kobayashi, J. Normand, K.

- Raghavachari, A. Rendell, J.C. Burant, S.S. Iyengar, J. Tomasi, M. Cossi, N. Rega, J.M. Millam, M. Klene, J. E. Knox, J. B. Cross, V. Bakken, C. Adamo, J. Jaramillo, R. Gomperts, R. E. Stratmann, O. Yazyev, A. J. Austin, R. Cammi, C. Pomelli, J. W. Ochterski, R. L. Martin, K. Morokuma, V. G. Zakrzewski, G.A. Voth, P. Salvador, J.J. Dannenberg, S. Dapprich, A. D. Daniels, O. Farkas, J. B. Foresman, J. V. Ortiz, J. Cioslowski, D. J. Fox, Gaussian 09, Revision A. 01, Gaussian Inc., Wallingford, CT, 2009.
- [33] C. Lee, W. Yang, R. G. Parr, Development of the Colle-Salvetti correlation-energy formula into a functional of the electron density, *Phys. Rev. B* 37 (1998) 785-789.
- [34] A. D. J. Becke, Density-functional thermochemistry. III. The role of exact exchange, *Chem. Phys.* 98 (1993) 5648-5652.
- [35] Tanaka M, Sekiguchi A. Hexakis(trimethylsilyl)tetrahydranyl tetrahydrane. *Angew. Chem. Int. Edit*, 44 (2005) 5821-5823.
- [36] P.R. Nambiar and S. R. Jain, Thermal characterization of tetramethylphosphonium perchlorate, nitrate and picrate, *Thermochimica Acta*, 9 (1974) 295-302.
- [37] A. Chandramohan, R. Bharathikannan, J. Chandrasekaran, P. Maadeswaran, R. Renganathan, V. Kandavelu, Synthesis, crystal growth and characterization of a new organic NLO material: Caffeinium picrate (CAFP) -A charge transfer molecular complex salt, *J. Cryst. Growth* 310 (2008) 5409-5415.
- [38] T. Dhanabal, G. Amirthaganesan, M. Dhandapani, Synthesis, spectral, thermal, optical and dielectric studies on 4-dimethylaminopyridinium picrate crystals, *Optik* 125 (2014) 4341-4346.
- [39] D. R. Kanis, M. A. Ratner, T. J. Marks, Design and construction of molecular assemblies with large second-order optical nonlinearities, *Chem. Rev.* 94 (1994) 195-242.
- [40] S. Manikandan, R. Mahalakshmi, P. Krishnan, F. Yogam, P. Rajesh, Growth, structural, optical, thermal and dielectric properties of l-asparagine monohydrate admixed l-thiomalic acid single crystal, *Optik*

127 (2016) 5316-5321.

[41] W. Wang, Y. Huang, N. Tang, Synthesis and infrared and fluorescence spectra of rare earth complexes with a novel amide-based ligand, *Spectrochim. Acta A* 66 (2007) 1058-1062.

[42] N. Elleuch, W. Amamou, A. B. Ahmed, Y. Abid, H. Feki, Vibrational spectroscopic study, charge transfer interaction and nonlinear optical properties of L-asparaginium picrate: A density functional theoretical approach, *Spectrochim. Acta A* 128 (2014) 281-289.

**Table 1** Crystallographic data for **1**

Compound	<b>1</b>
Empirical formula	C <sub>31</sub> H <sub>24</sub> PN <sub>3</sub> O <sub>7</sub>
Formula weight	581.50
Description	Pale Yellow, block
Crystal size (mm <sup>3</sup> )	0.13 × 0.17 × 0.21
Temperature (K)	291(2)
Wavelength (Å)	0.71073
<b>Crystal system</b>	Monoclinic
Unit cell dimensions	<i>P</i> 2(1)/ <i>c</i>
<i>a</i> (Å)	
<i>b</i> (Å)	9.950(1)
<i>c</i> (Å)	14.832(1)
$\beta$ (°)	19.576(2)
Volume (Å <sup>3</sup> )	103.93(1)
Z	2804.0(5)
Density (calculated, g cm <sup>-3</sup> )	4
Absorption coefficient (mm <sup>-1</sup> )	1.378
<i>F</i> (000)	0.152
$\theta$ range (°)	1208
Reflection collected	2.53 < $\theta$ < 26.5
Independent reflection ( <i>R</i> <sub>int</sub> )	26266
Data, restraints, parameters	5195 (0.038)
Goodness-of-fit on <i>F</i> <sup>2</sup>	5195, 0, 379
<i>R</i> <sub>1</sub> , <i>wR</i> <sub>2</sub> ( <i>I</i> > 2 $\sigma$ ( <i>I</i> ))	1.04
<i>R</i> <sub>1</sub> , <i>wR</i> <sub>2</sub> (all data)	0.0594, 0.1233
Largest diff. peak and hole (e Å <sup>-3</sup> )	0.0941, 0.1576
	0.76 and - 0.56

$$R_1 = \Sigma(|F_o| - |F_c|) / \Sigma|F_o|, wR_2 = [\Sigma w(|F_o|^2 - |F_c|^2)^2 / \Sigma w(|F_o|^2)^2]^{1/2}.$$

**Table 2** Selected bond parameters for **1**

Bond lengths (Å)		Bond Angles (°)	
O(2)–N(1)	1.173(6)	O(2)–N(1)–O(3)	119.5(3)
O(3)–N(1)	1.195(5)	O(4)–N(2)–O(5)	123.4(4)
O(4)–N(2)	1.219(6)	O(6)–N(3)–O(7)	122.3(4)
O(5)–N(2)	1.214(6)	O(2)–N(1)–C(2)	121.1(3)
O(6)–N(3)	1.207(5)	O(3)–N(1)–C(2)	119.4(4)
O(7)–N(3)	1.210(6)	O(4)–N(2)–C(4)	118.9(4)
O(1)–C(1)	1.233(4)	O(5)–N(2)–C(4)	117.7(4)
N(1)–C(2)	1.451(4)	O(6)–N(3)–C(6)	119.5(4)
N(2)–C(4)	1.445(6)	O(7)–N(3)–C(6)	118.3(3)
N(3)–C(6)	1.457(5)	C(13)–P(1)–C(19)	107.7(1)
P(1)–C(13)	1.814(3)	C(13)–P(1)–C(25)	110.2(2)
P(1)–C(19)	1.788(4)	C(13)–P(1)–C(31)	110.5(2)
P(1)–C(25)	1.798(3)	C(19)–P(1)–C(25)	109.1(2)
P(1)–C(31)	1.794(3)	C(19)–P(1)–C(31)	110.0(2)

**Table 3** Weak hydrogen bonds for **1** (Å and °)

D–H···A	<i>d</i> (D–H)	<i>d</i> (H···A)	<i>d</i> (D···A)	<(DHA)
C(7)–H(7)···O(6)	0.930	2.540	3.421(6)	158.0
C(13)–H(13A)···O(1)#1	0.970	2.320	3.128(4)	140.0
C(17)–H(17)···O(3)#2	0.930	2.490	3.286(6)	144.0
C(27)–H(27)···O(5)#3	0.930	2.560	3.187(6)	125.0
C(30)–H(30)···O(1)#1	0.930	2.370	3.163(4)	143.0

Symmetry transformations used to generate equivalent atoms: #1 =  $-x + 2, y - 1/2, -z + 1/2$ ; #2 =  $-x + 2, -y + 1, -z$ ; #3 =  $-x + 1, -y, -z$ ; #4 =  $x, -y + 2, z - 1/2$ .

**Table 4** Comparison of the first hyperpolarizability, polarizability, and dipole moment of **1** and its constituents calculated using DFT//B3LYP/6-31G(d, p)

Compounds	$\mu_{\text{tot}}$ (D)	$\alpha_{\text{tot}}$ ( $\times 10^{-24}$ esu)	$\beta_{\text{tot}}$ ( $\times 10^{-31}$ esu)
[PIC] <sup>-</sup> anion	2.61	17.3	75.10
[BzTPP] <sup>+</sup> cation	3.47	45.13	33.77
[BzTPP][PIC]	31.90	52.99	109.58

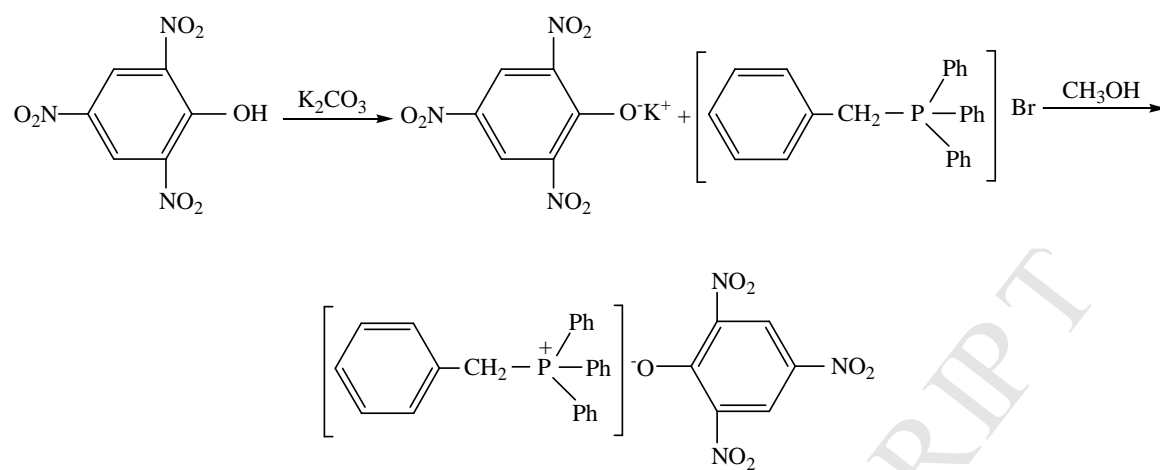


**Fig. 1.** Synthesis route of the title compound



**Fig. 2** Photograph of the title crystal grown by slow evaporation.

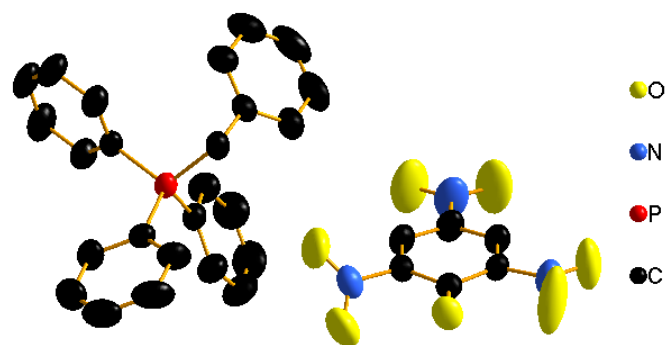
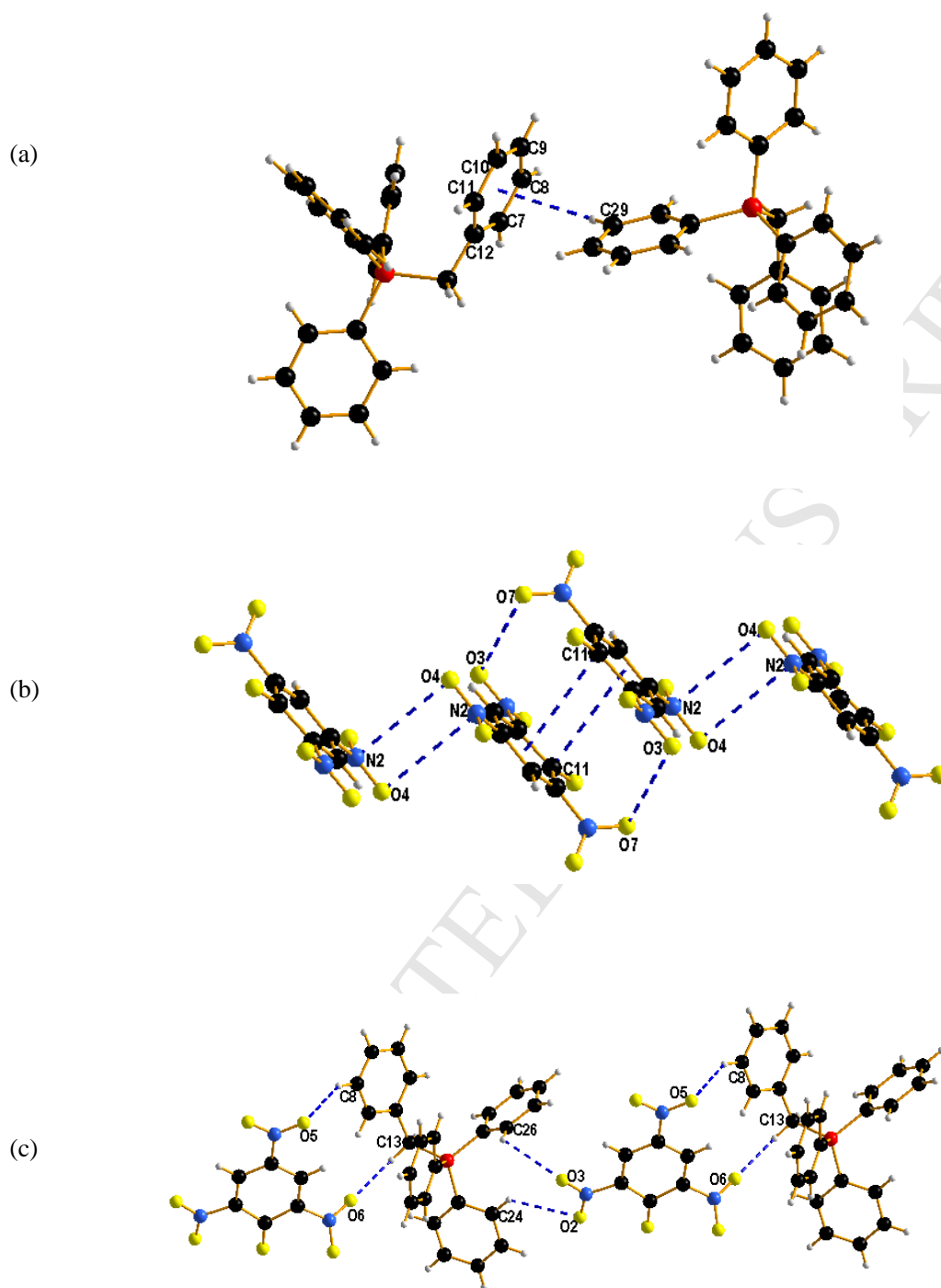
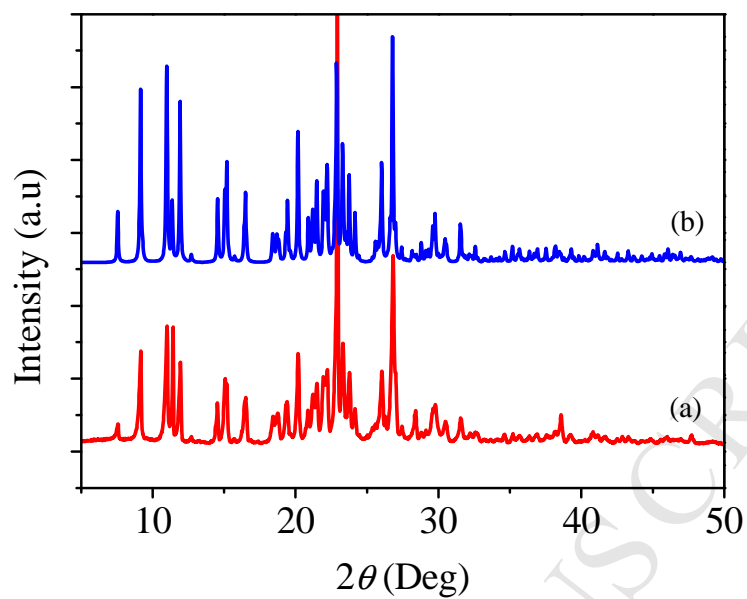


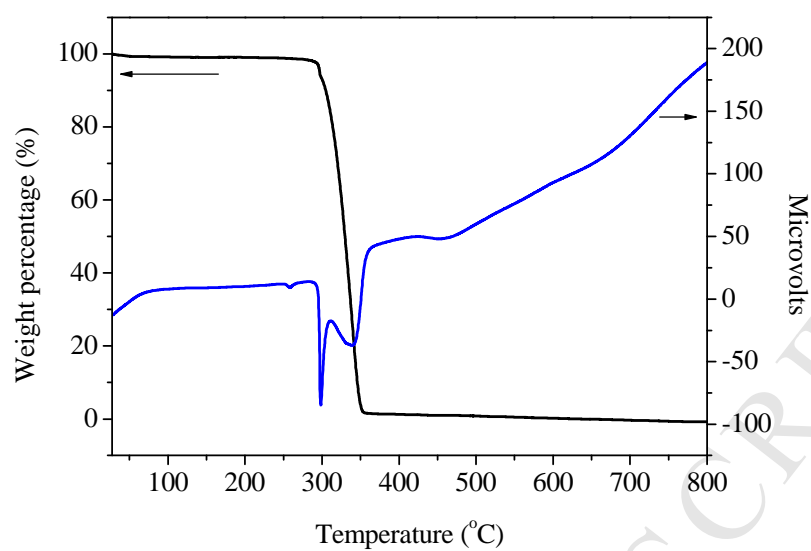
Fig. 3 ORTEP plot (30% probability ellipsoids) showing the molecule structure of **1**.



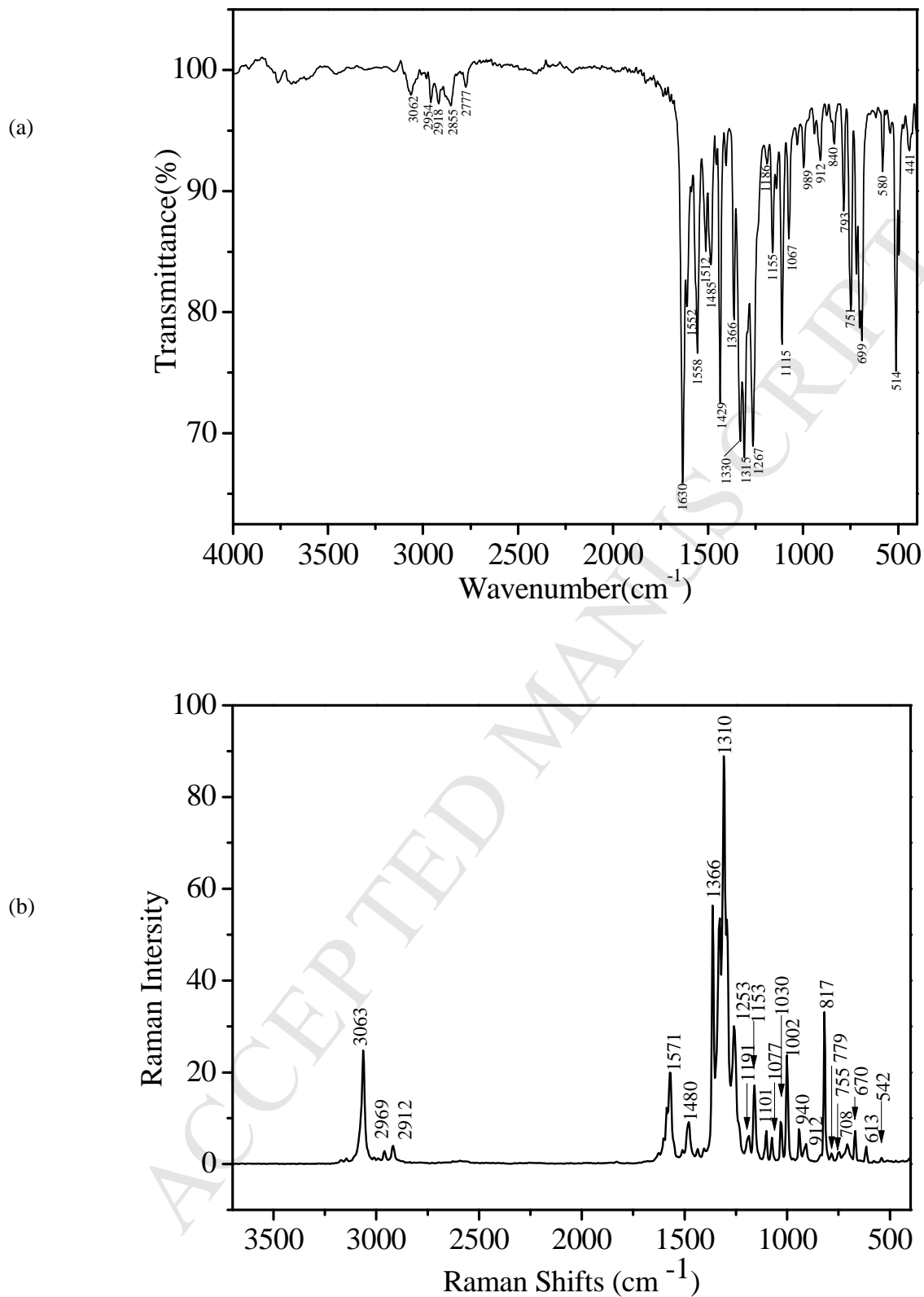
**Fig. 4** (a) The dimer formed through C-H... $\pi$  interaction between two neighboring [PIC]<sup>-</sup> anions of **1**. (b) The columnar structure formed through N-O, O-O and  $\pi$ ... $\pi$  interactions between the cations of **1**. (c) The anion and cation formed an alternating network structure in a ...ACACAC... sequence through C-H...O hydrogen bonds of **1**.



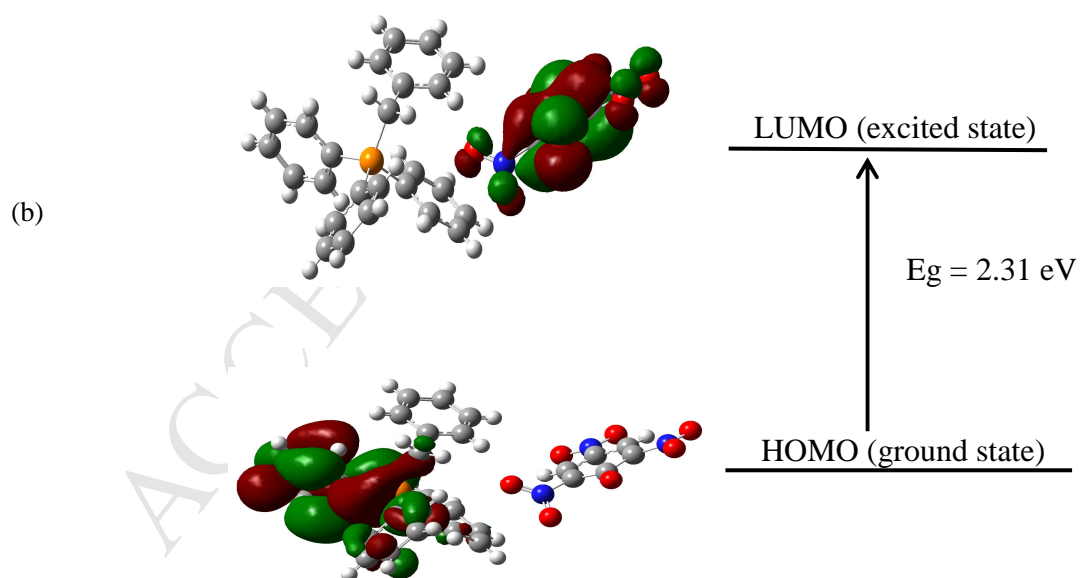
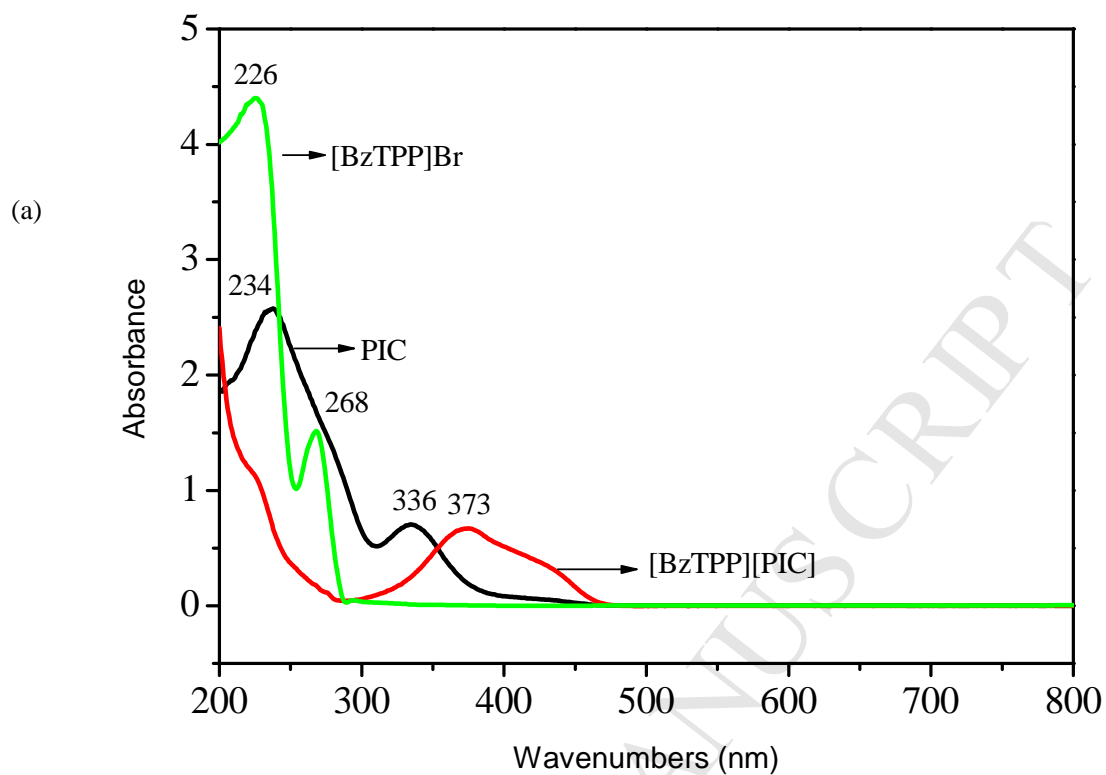
**Fig. 5** Simulated and experimental powder XRD patterns of **1**: (a) experimental (red line) and (b) calculated from single crystal structural analysis (blue line).



**Fig. 6** TG-DTA thermal curve for **1**.



**Fig. 7** The FT-IR (a) and Raman (b) spectra of **1**.



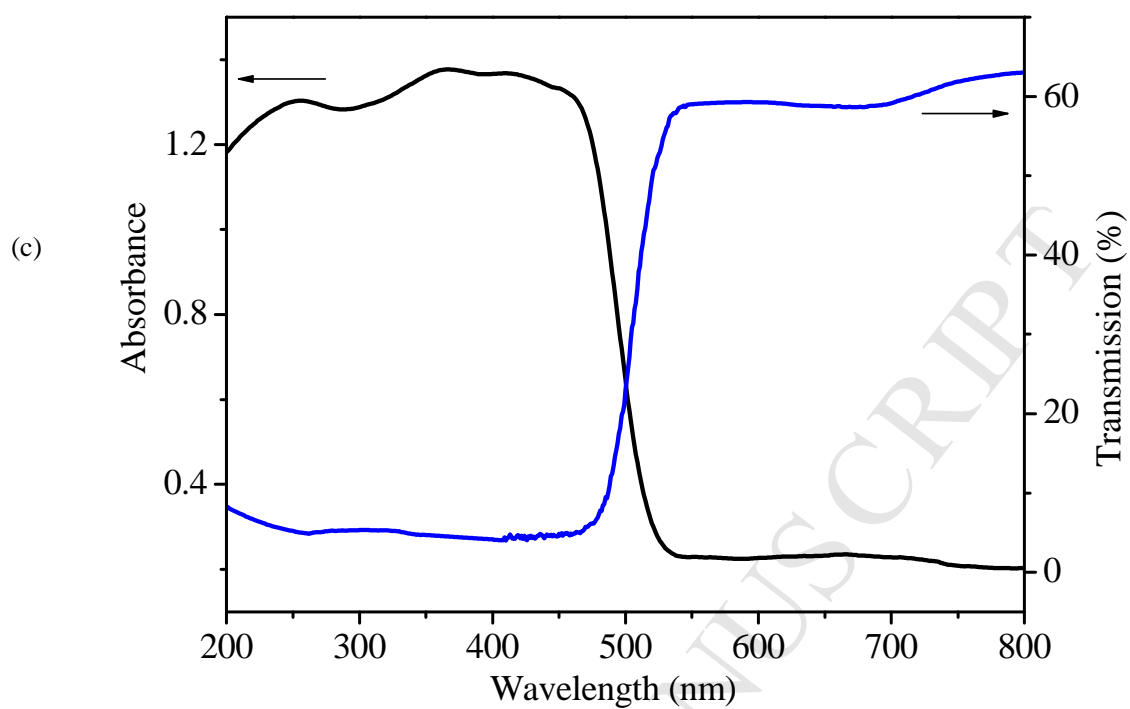


**Fig. 8** (a) UV-Vis absorption spectrum of **1** (red), intermediate [BzTPP]Br (blue) and piric acid (black). (b) HOMO-LUMO energy gap of **1**. (c) The absorbance and transmission spectra of **1** in the solid state.

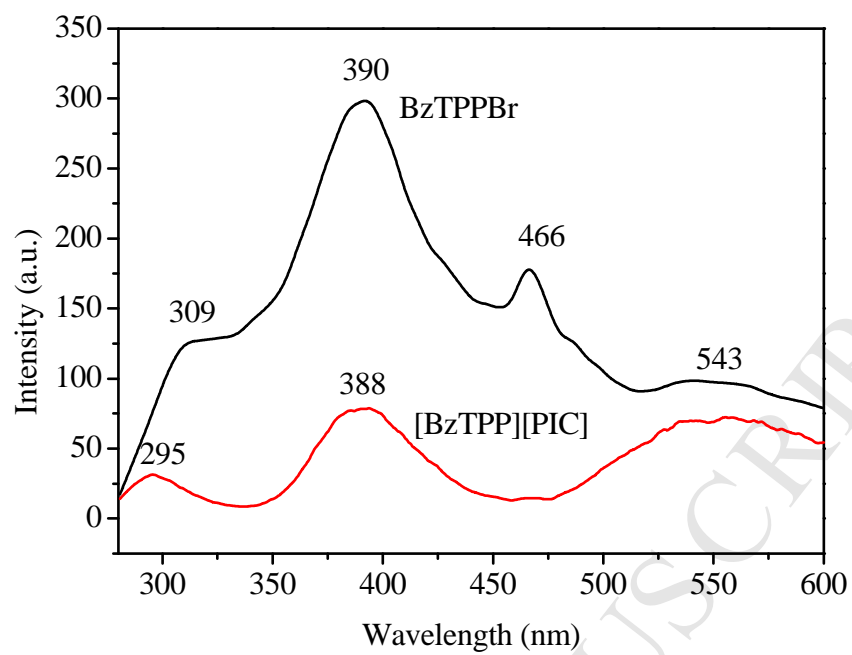


**Fig.9** Emission spectra of **1** (red) and [BzTPP]Br (black) in the solid state at room temperature.

## Research Highlights

1. A organic crystal of benzyl triphenylphosphinium picrate salt was synthesized and characterized.
2. The detailed interpretation of IR and Raman spectra and emission spectra of the crystal was reported.
3. The thermal stability of the organic crystal was analyzed by TG-TDA-MS technique.
4. The HOMO-LUMO energy gap explains the charge transfer interactions in the molecule.
5. The energy of weak interactions in the molecule and nonlinear optical properties were studies using DFT calculations.
6. The title crystal show main emission peaks about 295, 388 and 543 nm in solid state at room temperature.